A Broadband Technique for a Decoupling Network in a Compact Antenna Array in a MIMO System

Jung H. Ko,[*] **Jung H. Han, and Noh H. Myung**

Abstract—Decoupling networks (DNs) have frequently been used to obtain high isolation performance between coupled antennas in multiple-input multiple-output (MIMO) systems due to their advantage of spatial efficiency, which is particularly important for mobile devices. However, conventional DNs suffer from narrowband limitations. In this paper, a broadband decoupling technique is proposed that broadens the isolation bandwidth using a parallel resonant point. A 1.95 GHz MIMO antenna system with 460 MHz of bandwidth (fractional bandwidth, FBW = 23.6%) is designed and measured using the scattering parameters. The isolation is found to be better than -15 dB, while the reflection coefficient is better than -6 dB. Furthermore, the antenna efficiency and envelope correlation coefficient (ECC) are evaluated in a reverberation chamber.

1. INTRODUCTION

In recent years, wireless communication systems need to accommodate higher data rates. In particular, the long-term evolution (LTE) network has been developed to provide better performance for mobile communication systems. As a key technology for the spatial diversity techniques in LTE system, the multiple-input multiple-output (MIMO) scheme has been investigated widely. MIMO technology provides good quality of service (QoS) in multi-path environments without requiring additional power [1–3]. It is an effective method of improving the reliability of communications and increasing the channel capacity. For a $N_r \times N_t$ MIMO system, as long as the multiple channels are independent of each other, the data throughput can be increased $N_{\min}$ times, where $N_{\min} = \min(N_r, N_t)$ [4]. However, it is not easy to place multiple antennas in a mobile handset that has limited space. Because the MIMO antenna elements in recent mobile handsets are collocated on the printed circuit board (PCB), the surface current distribution on the PCB induces mutual coupling between the antenna elements and common ground plane. Furthermore, because the multiple antennas are closely placed, the coupling between them becomes stronger and signal leakage occurs from one antenna to another. Then, the signal correlations increase among the multiple channels. Consequently, the diversity or channel capacity of the MIMO antenna system is significantly degraded. Therefore, in portable MIMO devices where antennas must be designed within a small space, it is important that low correlation and high isolation between closely space antennas is achieved [5].

Over the years, there have been numerous studies that focused on reducing the coupling of antennas. Electromagnetic band gap (EBG) structures have been used to diminish this coupling [6, 7]; however, these structures are complicated and require a large structure. In [8–11], mutual coupling was reduced using etching slits and slots on the ground plane called a defected ground structure (DGS), but sometimes a large ground plane was required in order to achieve this reduction. Furthermore, DGS systems have disadvantages in practical implementation due to their complicated ground structures. Port decoupling can also be achieved using suspended metal strip lines that cancel the reactive coupling

The authors are with the Department of Electrical Engineering, Korea Advanced Institute of Science and Technology (KAIST), 291 Daehak-ro, Yuseong-gu, Daejeon 305-701, Korea.

between antennas, and this is referred to as a neutralization technique [12, 13]. However, this method requires an extensive load in the iterative computation procedure in order to determine the length and appropriate points on the elements, and it also has the disadvantage of a narrow bandwidth.

A correlation reduction technique with a negative group delay using slots was proposed for compact MIMO systems in [14]. When two linearly polarized antennas are located orthogonally to each other, they can reduce the mutual coupling and provide polarization diversity [15, 16]. However, they require a large antenna space and ground. In [17], a MIMO antenna was designed with a low correlation over the broadband frequencies. However, the antenna spacing between the two antennas was larger than the half-wavelength, which indicates that they were not closely spaced.

A microstrip-based hybrid coupler can also be used to obtain decoupled ports [18], but it is not suitable for small handset applications due to its bulky size in realization, and it also has a narrow bandwidth. In [19, 20], broadband performance was obtained using a hybrid coupler, but these couplers required too much space. In order to overcome the problems associated with their large size, an LC-based hybrid coupler was used [21], but it had a narrow bandwidth performance. A decoupling design was investigated through adding a hybrid coupler in [22]. However, it also had a narrow bandwidth.

Finally, in [23–26], a decoupling network (DN) was proposed for MIMO systems in order to obtain high isolation between two antenna ports within a small space. DNs have been frequently used due to their advantage of spatial efficiency, which is particularly important for mobile devices. However, conventional DNs also have a disadvantage of a narrow bandwidth.

In this paper, a broadband technique is proposed, which is suitable for small spaces such as mobile devices and that broadens the bandwidth of the DN.

2. PROPOSED BROADBAND DECOUPLING TECHNIQUE

Figure 1 presents a block diagram of a MIMO antenna system with a DN. The DN consists of a T-line with a characteristic impedance Z_0 $(= 50\,\Omega)$ and electrical length θ at each port and a shunt reactive component with an admittance jB_d. When the MIMO antenna is assumed with good input matching at each port at the center frequency, the scattering matrix of the MIMO antenna can be described as follows:

$$S^a = \begin{bmatrix} 0 & \alpha e^{j\varphi} \\ \alpha e^{j\varphi} & 0 \end{bmatrix}, \tag{1}$$

where α and φ are the magnitude and phase of the coupling coefficient among antennas, respectively. Through adding a T-line with the same impedance Z_0 to each port, the scattering matrix at reference plane b can be expressed as follows:

$$S^b = \begin{bmatrix} 0 & \alpha e^{-j(2\theta-\varphi)} \\ \alpha e^{-j(2\theta-\varphi)} & 0 \end{bmatrix}, \tag{2}$$

and the corresponding admittance matrix can be easily derived [27], as shown below:

$$Y^b = \frac{Y_0}{\{1-\alpha^2 e^{-j2(2\theta-\varphi)}\}} \begin{bmatrix} 1+\alpha^2 e^{-j2(2\theta-\varphi)} & -2\alpha e^{-j(2\theta-\varphi)} \\ -2\alpha e^{-j(2\theta-\varphi)} & 1+\alpha^2 e^{-j2(2\theta-\varphi)} \end{bmatrix}, \tag{3}$$
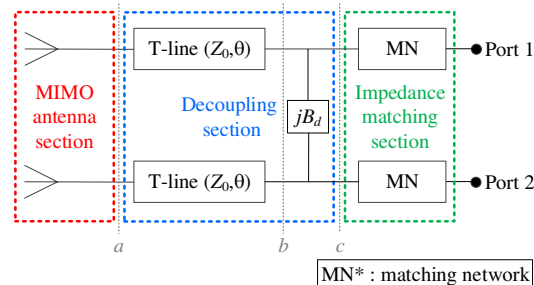

Figure 1. Block diagram of a MIMO antenna system with a decoupling network.

where the Y_0 represents the characteristic admittance, $Y_0 = 1/Z_0$. With a shunt reactive component jB_d, the admittance matrix Y^c can be expressed as follows:

$$Y^c = \frac{Y_0}{\left\{1 - \alpha^2 e^{-j2(2\theta-\varphi)}\right\}} \begin{bmatrix} 1 + \alpha^2 e^{-j2(2\theta-\varphi)} & -2\alpha e^{-j(2\theta-\varphi)} \\ -2\alpha e^{-j(2\theta-\varphi)} & 1 + \alpha^2 e^{-j2(2\theta-\varphi)} \end{bmatrix} + \begin{bmatrix} jB_d & -jB_d \\ -jB_d & jB_d \end{bmatrix}. \quad (4)$$

When the T-lines with length θ at each port have the values in Equation (5), the transadmittance Y_{21}^b becomes purely imaginary. Through adding the reactive component jB_d, which has the value described in (5), the transadmittance Y_{21}^c can be removed.

$$\theta = \frac{1}{2}\left(\varphi \pm \frac{\pi}{2}\right), \quad B_d = \pm\frac{2\alpha}{1+\alpha^2}Y_0 \quad (5)$$

Then, the coupling coefficient S_{21}^c moves to zero; that is, the two ports are decoupled, as seen in Equation (6) [27]:

$$S_{21}^c = \frac{-2Y_{21}^c Y_0}{Y_0{}^2 + 2Y_{11}^c Y_0 + (Y_{11}^c)^2 - (Y_{21}^c)^2}. \quad (6)$$

Next, a further impedance matching network is required in order to transfer the input admittances (Y_{11}^c and Y_{22}^c) to the system admittance Y_0.

From (5), it can be found that once a MIMO antenna is designed, there are two possible DNs that correspond to the designed antenna: a positive B implies a capacitor and a negative B indicates an inductor. Because a positive B corresponds to a positive θ, which means a shorter length of T-lines, a capacitor is preferred in the conventional DN [25]. However, the conventional DN suffers from the narrow-band limitation because the transadmittance (and coupling coefficient) of the MIMO system cannot be removed effectively when the length of the T-line is too short. In order to overcome this narrow-band characteristic, it is necessary to consider a resonance type of antenna system and variations of the imaginary part of the transadmittance, or trans-susceptance (Im[Y_{21}]). The MIMO antenna section at the reference plane a is assumed to be well matched at desired center frequency at each port. After adding T-lines (Z_0, θ) at each port, the transadmittance (or transimpedance) of the MIMO antenna with a decoupling section at b changes while the matching performance is maintained. Equations (2) and (3) indicate mathematically that as the T-line increases in length, the complex value of the transadmittance Y_{21}^b is changed, whereas the absolute values of the scattering parameters are invariant.

In [28], variations of the input reactance versus frequency for a single monopole antenna were well described in terms of the resonant phenomena. As shown in [28, see Chapter 4.7.4], there are two resonance types. The first resonance type is a series with slowly varying values of reactance versus frequency, and it has a desirable magnitude for practical implementation. For frequencies below the series resonance, the impedance is capacitive (i.e., the imaginary part is negative) and above the series resonance, the impedance is inductive (i.e., the imaginary part is positive). The second resonance type is parallel; that is, it is anti-resonance with large and rapid changes in the values of the reactance. For frequencies below the parallel resonance, the impedance is inductive and above the parallel resonance, the impedance is capacitive. That can extend to a multiple antenna case and is summarized in Table 1.

Therefore, the MIMO antenna section at reference plane a is a series resonant circuit. Furthermore, depending on the length of the added T-line, the MIMO system at reference plane b can be considered

Table 1. Comparison of the parameter characteristics corresponding to the antenna resonance type.

Resonance type	Impedance below the resonant frequency	Impedance above the resonant frequency	Variation of input reactance	Variation of trans-susceptance
Series	Capacitive $(-jX)$	Inductive $(+jX)$	Slow	Rapid
Parallel	Inductive $(+jX)$	Capacitive $(-jX)$	Rapid	Slow

as a series resonant circuit or a parallel resonant circuit, or neither. Because the isolation or decoupling effect, which is the elimination of the remaining purely imaginary value of transadmittance, is obtained through adding a shunt reactive component, the isolation performance is strongly affected by the cancellation range of the trans-susceptance. That is, the smaller the fluctuation of the trans-susceptance, the wider the isolation bandwidth.

A simple printed monopoles MIMO antenna was designed at 1.95 GHz, which was simulated on a 1 mm thick FR-4 substrate with a relative permittivity of 4.9, as shown in Figure 2(a). It was assumed that the target bands were from 1.7 GHz to 2.2 GHz. The MIMO antenna was an antenna (with a conventional DN) for comparison and not a proposed antenna. The simulated results were obtained using two software tools: the High Frequency Structure Simulator (HFSS) and the Advanced Design System (ADS). The coupling coefficient (S_{21}) at 1.95 GHz had a phase $\varphi = -52.8°$. From (5), the required T-line length was either $\theta = 18.6°$ (4.19 mm) or $\theta = 108.6°$ (24.39 mm). Therefore, one of these two values was chosen as the T-line length for the conventional scheme.

In Figure 2, the relationship between the input reactance and trans-susceptance variation depending on the length of the T-lines is shown. In Figure 2(a), it is seen that the MIMO antenna without T-lines is a series resonant circuit, and it has a rapid variation of trans-susceptance below the center frequency. The maximum difference of the trans-susceptance within the target bands was approximately 0.07 (Ω^{-1}). In Figure 2(b), it was found that the MIMO antenna for the conventional scheme with short T-lines was also a series resonant circuit, and it had more rapid variations of trans-susceptance below the center frequency. The maximum difference of the trans-susceptance within the target bands was approximately 0.09 (Ω^{-1}). However, in Figure 2(c), a parallel resonance occurred near 1.9 GHz for the conventional scheme with long T-lines, and the variation of the trans-susceptance above the center frequency was large. Therefore, the maximum difference of the trans-susceptance within the target bands remained approximately 0.09 (Ω^{-1}).

However, it is expected that the variation of the trans-susceptance was significantly better (i.e., smaller), when the T-line length was appropriately determined within the two solutions (4.19–24.39 mm). With 20.1 mm long T-lines at each port, the parallel resonance occurred at the center frequency, and the variation range was within 0.01, as shown in Figure 2(d). In this case, the remaining trans-susceptance was effectively removed through adding a shunt reactive component. This resulted in the broadband isolation performance. Therefore, through using this characteristic, a MIMO antenna system was designed with a broadband decoupling network.

3. MIMO ANTENNA DESIGN WITH A BROADBAND DECOUPLING NETWORK

A prototype MIMO system was designed with a broadband decoupling network; this was also simulated and measured. The proposed MIMO system was fabricated on a 1 mm thick FR-4 substrate with a relative permittivity of 4.9 and a size of $50 \times 100 \, \text{mm}^2$, which is suitable for mobile handset devices and is the same size as the antenna in Figure 2. The system can be divided into three sections: a MIMO antenna section, a broadband decoupling section, and a broadband impedance matching section.

First, a MIMO antenna that consisted of two printed meander-line monopoles with a spacing $S = 24.8 \, \text{mm}$ ($0.16\lambda_0$ at 1.95 GHz) is proposed. The configuration of the MIMO antenna section and the simulated S-parameters are presented in Figure 3 and Figure 4, respectively. It can be seen that the MIMO antenna has $-6 \, \text{dB}$ impedance bandwidths of 460 MHz (1710–2170 MHz, 23.6%), which covers LTE bands 1, 2, 3, 4, 9, 10, and 25. However, because the antenna spacing is much shorter than the half-wavelength of the center frequency, the coupling coefficient between the antennas was almost $-6 \, \text{dB}$, which is not sufficient for decoupling between two antennas.

In order for the broadband decoupling section to achieve better isolation performance over the broadband frequency region, T-lines with a length 17.7 mm ($\theta = 78.8°$) at each port and a shunt inductor (3.3 nH) were adopted. The resultant trans-susceptance and S-parameters are illustrated in Figure 5. A MIMO antenna with a conventional DN was also simulated in order to compare the isolation bandwidths of the two antennas. The conventional scheme consisted of the MIMO antenna in Figure 2(a) and a conventional DN with two 4.19 mm T-lines (Figure 2(b)) and a shunt capacitor (1.5 pF). As seen in Figure 5(a), although the conventional scheme removed the trans-susceptance at the center frequency, the remaining values of the trans-susceptance over the target bands were too large.
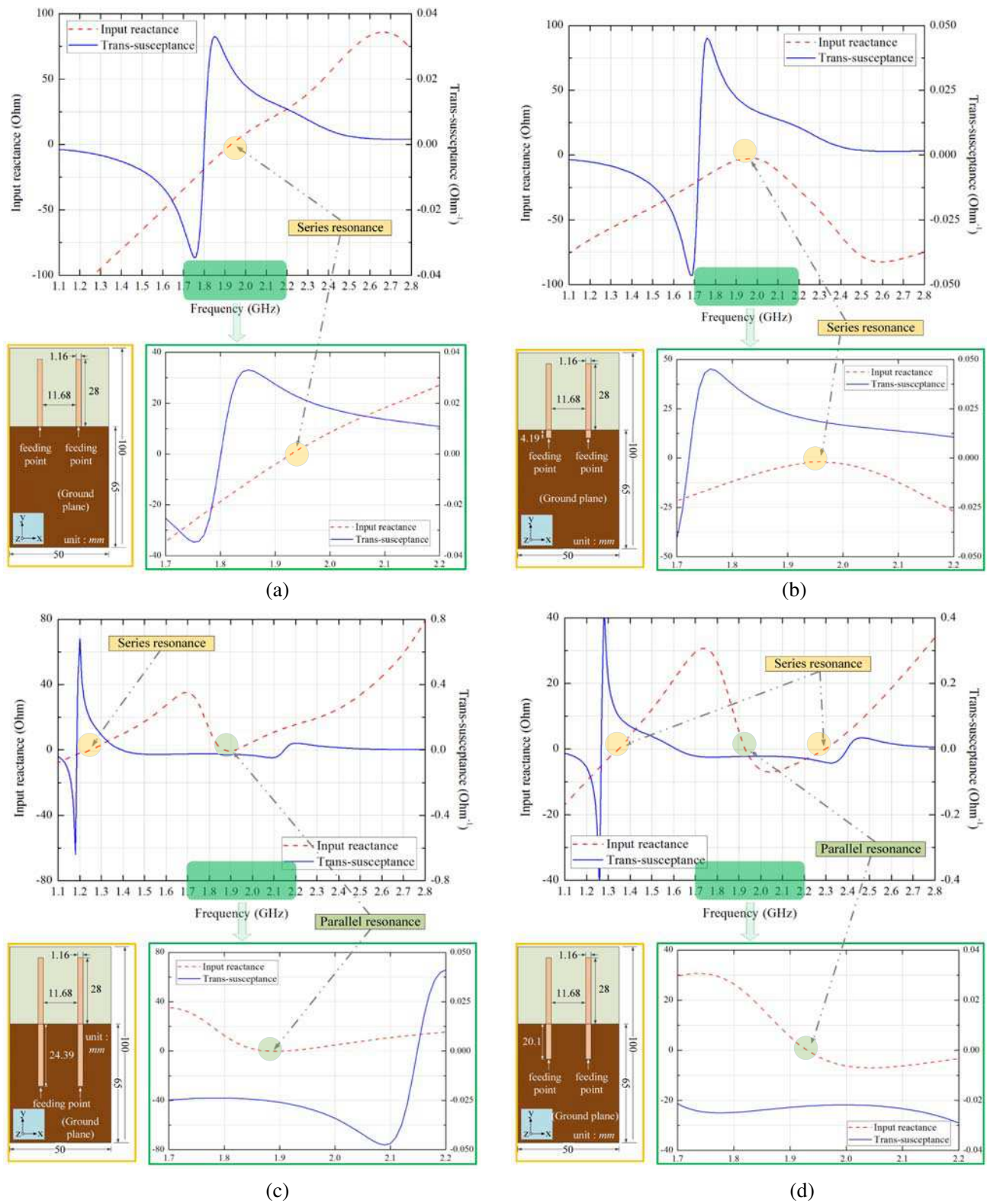
Figure 2. Relationship between the input reactance and trans-susceptance for a MIMO system at 1.95 GHz: (a) without T-lines, (b) with T-lines ($\theta = 4.19$ mm), (c) with T-lines ($\theta = 24.39$ mm), and (d) with T-lines ($\theta = 20.1$ mm).
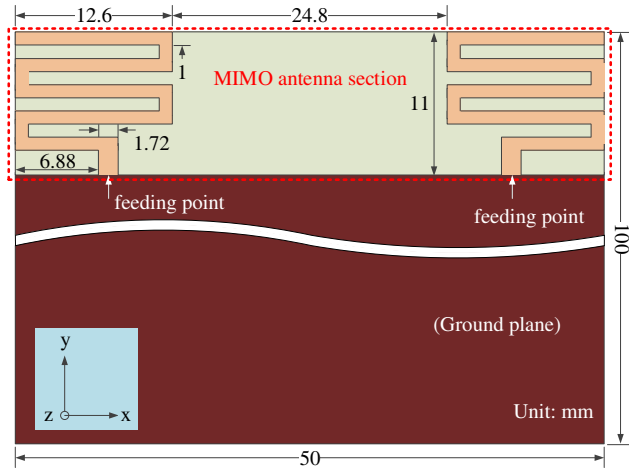
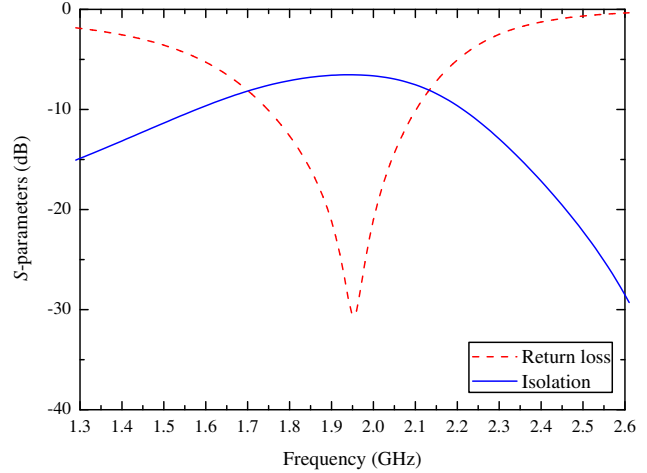**Figure 3.** Proposed MIMO antenna.

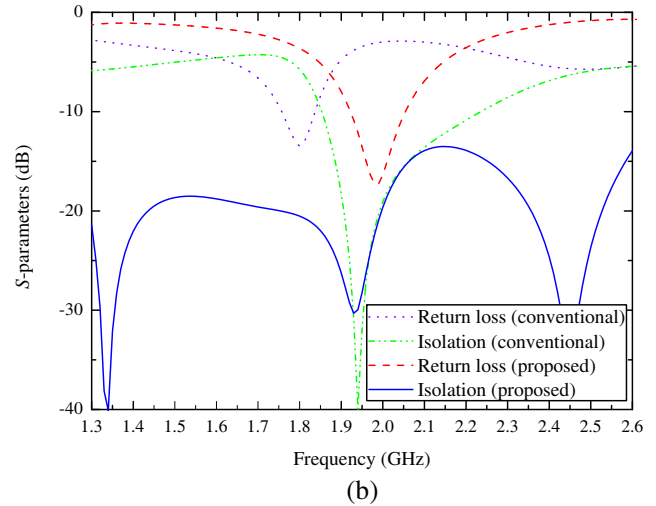**Figure 4.** S-parameters in the simulation for the proposed MIMO antenna section.
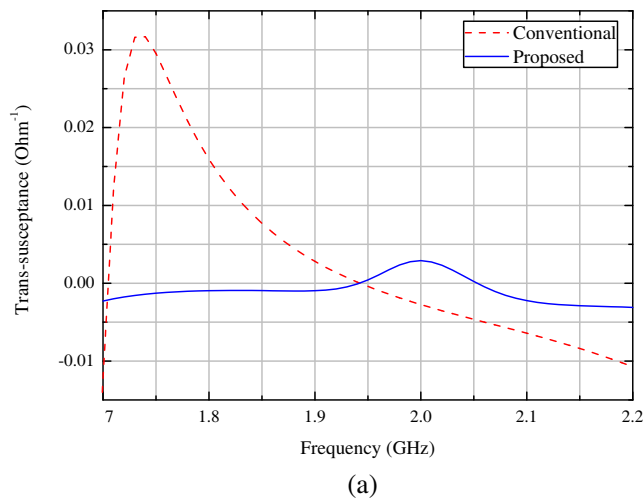

(a)

(b)

Figure 5. MIMO system after both conventional and proposed decoupling networks (without matching networks): (a) trans-susceptance in simulation and (b) the simulated S-parameters.

In contrast, the proposed DN exhibited almost-zero values of trans-susceptance for the entire target bands, which resulted in broadly isolated performance. In Figure 5(b), it can be seen that the coupling coefficients of the proposed system were lower than -15 dB throughout the target bands (460 MHz), while the conventional scheme had -15 dB isolation bandwidths of only 150 MHz.

Finally, an impedance matching network was required in order to equalize the input admittances after adding the decoupling network to the system admittance (Y_0). Conventionally, a conjugate-matching technique is used. However, this technique has a narrow-band matching performance, and thus a broadband matching technique is required for the proposed system. In this paper, the simplified real frequency technique (SRFT) was used, because it does not require an equivalent load model and only requires the measured or simulated impedance data [29]. After an optimization process using the ADS simulation tool, a 1.8 pF series capacitor and a 2.7 nH shunt inductor were used at each port. The configuration of the proposed MIMO system and the resultant S-parameters are shown in Figure 6 and Figure 7, respectively. In order to compare the proposed scheme with a conventional scheme, a conventional MIMO system was also simulated. For the impedance matching network in the conventional system (the conjugate-matching technique), a 1.7 nH series inductor and a 3 nH shunt
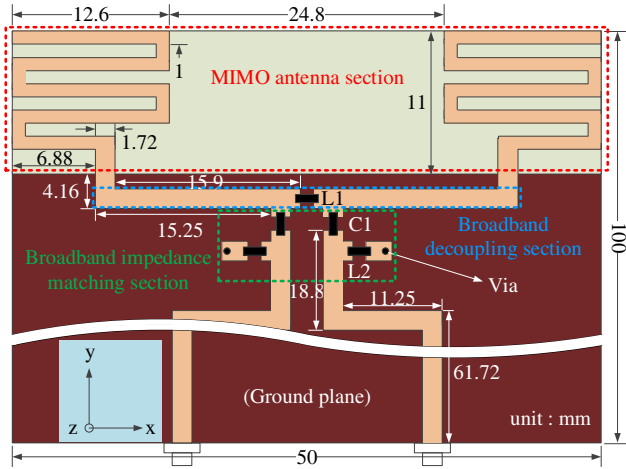
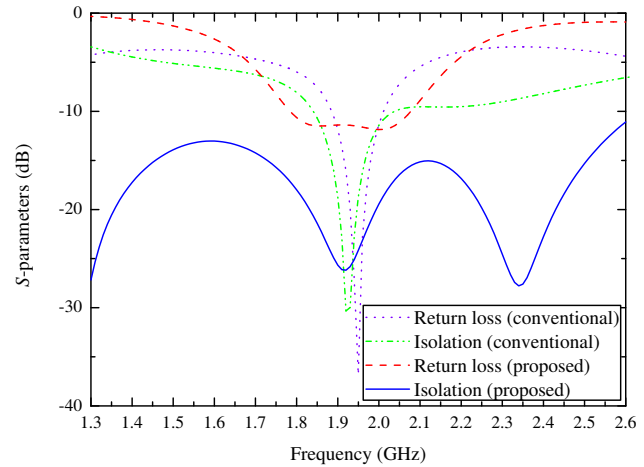**Figure 6.** Proposed MIMO system with broadband decoupling and matching networks.

Figure 7. Simulated S-parameters after both conventional and proposed decoupling and matching networks.
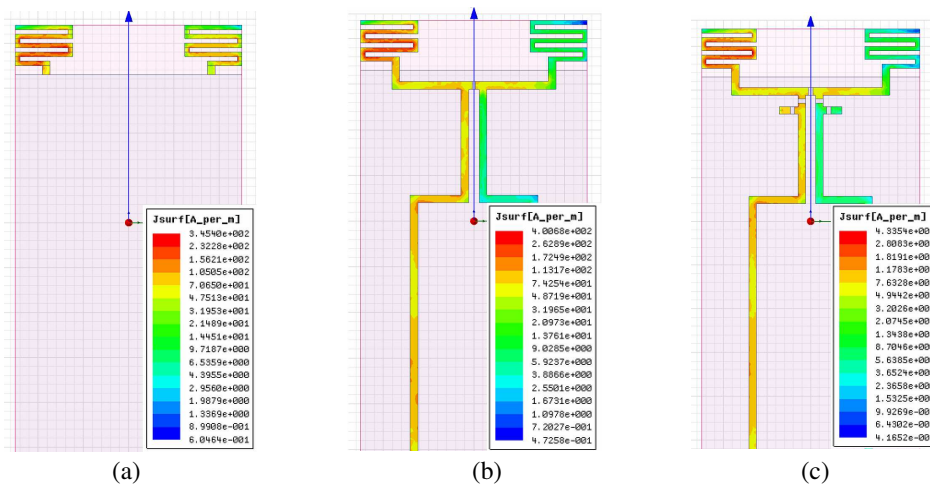

Figure 8. Simulated surface current magnitudes at 1.95 GHz: (a) MIMO antenna only section, (b) MIMO antenna with broadband decoupling section, and (c) MIMO antenna with broadband decoupling and impedance matching section.

inductor were adopted at each port. The conventional scheme had bandwidths of only 100 MHz that satisfied the -6 dB return loss and -15 dB isolation performances in the target bands. However, the proposed MIMO system with the broadband decoupling network had 460 MHz bandwidths, which were sufficient to fulfill the requirements.

Figure 8 presents the surface current distributions of the three cases: MIMO-only antenna section, MIMO with decoupling network, and MIMO with decoupling and matching networks. From the results, it is clearly seen that the antenna coupling effect is well suppressed through the addition of the decoupling network, whereas the antenna only section exhibits a severe coupling effect.

Photographs of the fabricated proposed MIMO system and measurement S-parameters are presented in Figure 9 and Figure 10, respectively. It is seen that the measurements agree with the simulated results well.

In Table 2, the performance and size of the proposed MIMO system are compared with those of some published research works explained in Section 1. The proposed system is compact, and it broadens
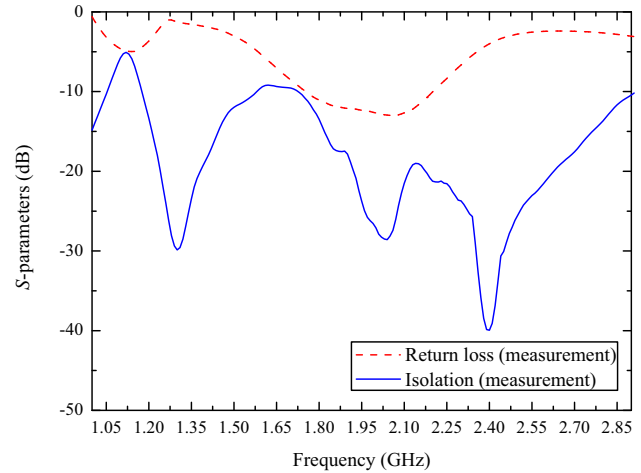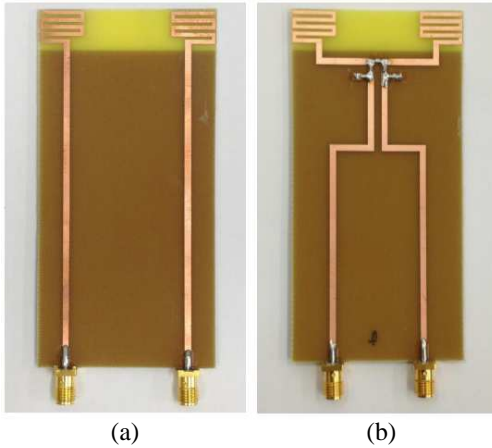
(a)   (b)

Figure 9. Photographs of the fabricated antennas: (a) the proposed MIMO antenna and (b) the entire proposed MIMO system.

Figure 10. Measured S-parameters for the proposed MIMO system.

Table 2. A comparison table that compares the performance and size of the proposed MIMO system with other published research works.

Decoupling techniques	Electromagnetic Band Gap [7]	Defected Ground Structure [11]	Negative Group Delay [14]	Widely separated antennas [17]		Microstrip hybrid coupler [22]	LC-based hybrid coupler [21]	Conventional Decoupling Network [25]	Proposed broadband Decoupling Network
Center frequency [GHz]	2.5	2	0.74	1.8	2.6	2.4	0.71	2.45	1.95
Antenna spacing [mm]	35.5	26	5	88		10	8	8.5	24.8
Decoupling elements (Size [mm²])	EBG (29×72.5)	Slits and Slots (20×20)	Slits	–		Ring hybrid (20×30)	T-lines & LC components	T-lines & LC components	T-lines & LC components
MIMO system size [mm²]	84×72.5	50×63	40×100	58×118		22×59	50×110	22×67.5	50×100
Bandwidth [MHz] ($S_{11} < -6$ dB, $S_{21} < -15$ dB)	850	950	10	50	100	100	100	100	460

the bandwidth of the conventional DN and other narrow-band techniques.

The measured radiation patterns of the proposed MIMO system at 1.95 GHz are illustrated in Figure 11. Figures 11(a), 11(c), and 11(e) are the patterns with port 1 excited and port 2 terminated to a 50 Ω load, and the other images are the reverse. The patterns of the two antennas are symmetric.
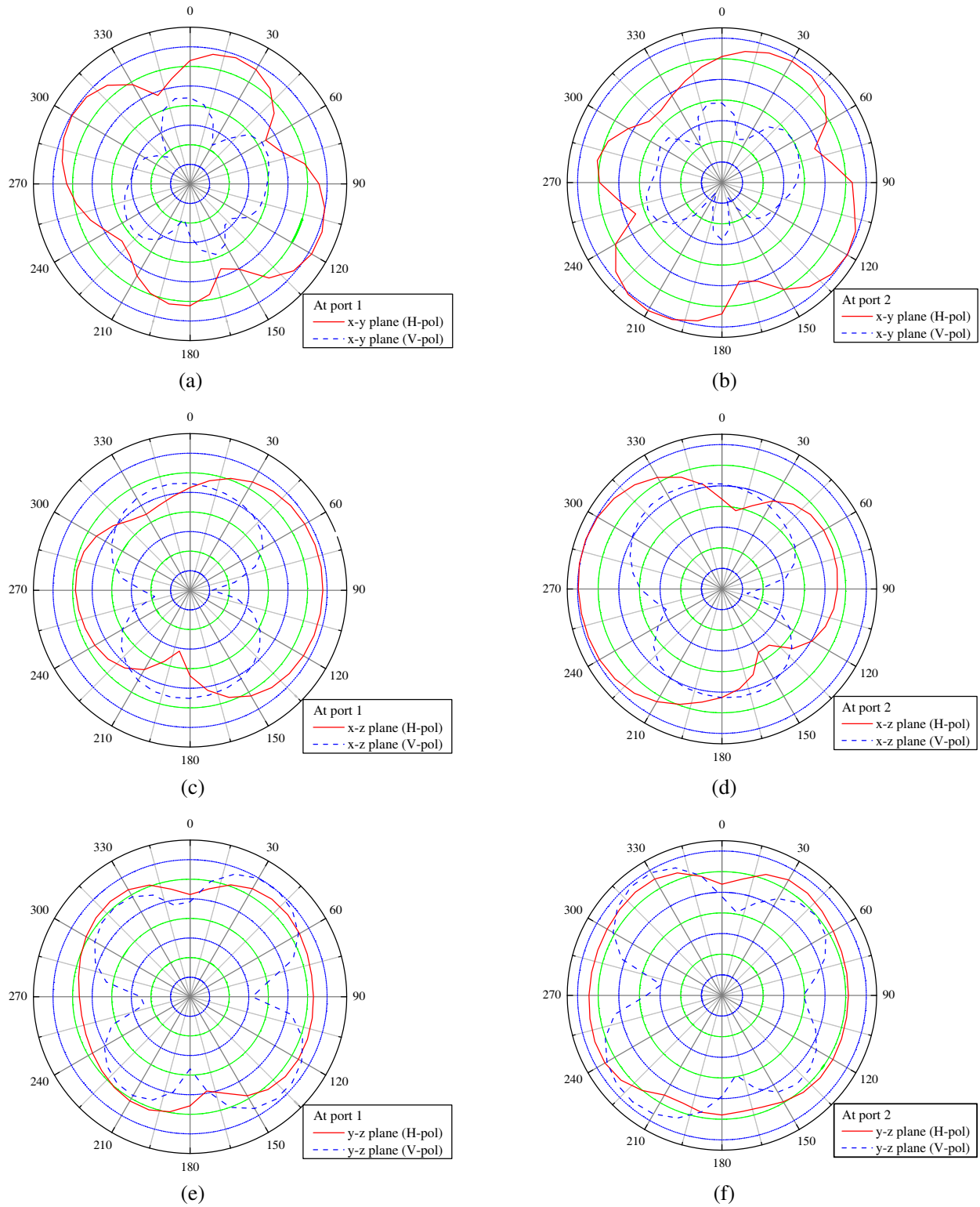
Figure 11. Measured radiation patterns of the proposed system at 1.95 GHz: (a) x-y plane at port 1, (b) x-y plane at port 2, (c) x-z plane at port 1, (d) x-z plane at port 2, (e) y-z plane at port 1, and (f) y-z plane at port 2.

4. MIMO SYSTEM PERFORMANCE EVALUATION

In order to evaluate the performance of the proposed MIMO system, the antenna efficiency and envelope correlation coefficient (ECC) were measured in a reverberation chamber (RC), which had dimensions of $1.94 \times 2.0 \times 1.4 \, \text{m}^3$. The RC can generate a Rayleigh distribution as multi-path fading in real communication environments through rotating a mode stirrer. For comparison, the proposed MIMO antenna (antenna only) and the MIMO system with a broadband DN (Figure 9) were tested.

The antenna efficiencies of two cases are shown in Figure 12. It is clearly seen that the proposed MIMO system (with the broadband DN) had better performance than the MIMO antenna without the broadband DN within the target bands. Without the broadband DN, the MIMO antenna had efficiencies of 50–65% over the target bandwidth. With the broadband DN, the efficiencies of antennas 1 and 2 were from 65% to 80% over the desired bandwidth.

Another significant factor in evaluating the performance of MIMO systems is the ECC whose equation is described below [30]:

$$R = E\left[vec\left(H\right) vec(H)^*\right]$$
$$\rho_{env} = \left| \frac{R\left(1,2\right)}{\sqrt{R\left(1,1\right) R\left(2,2\right)}} \right|^2, \tag{7}$$

where H is the normalized measured channel matrix obtained using the Frobenius norm, $E[\cdot]$ the statistical expectation taken from the samples of the channel matrix, and * indicates a complex conjugate transpose. The ECCs with and without the broadband DN are illustrated in Figure 13. It was found that a MIMO with the broadband DN exhibited a lower correlation over the desired frequencies compared with the MIMO antenna without the broadband DN. For the MIMO antenna only, the ECC values were within from 0.25 to 0.45; whereas they were lower than 0.22 over the desired bandwidth for the proposed MIMO system.
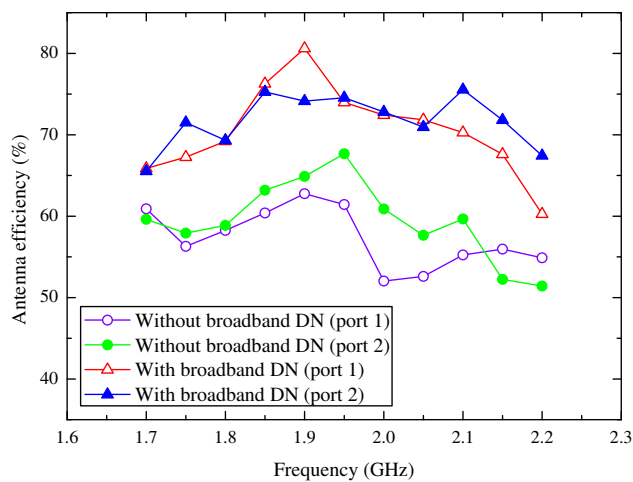

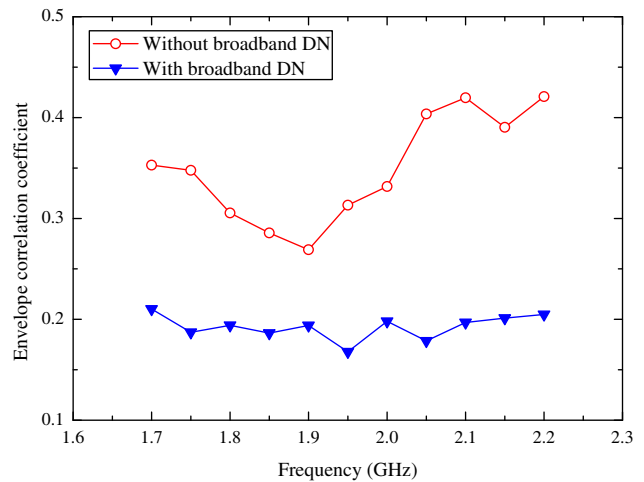**Figure 12.** Antenna efficiencies measured in a reverberation chamber.

Figure 13. Envelope correlation coefficient measured in a reverberation chamber.

5. CONCLUSION

In this paper, a broadband decoupling technique between two closely spaced antennas ($0.16\lambda_0$ at 1.95 GHz) was developed. This technique improved the conventional DN in terms of the bandwidth performance through analyzing the type of resonance in the MIMO antenna. The proposed MIMO system is simple and compact, and it achieves $-6 \, \text{dB}$ impedance bandwidth and $-15 \, \text{dB}$ isolation bandwidth in frequencies from 1710 MHz to 2170 MHz. The prototype MIMO system was also evaluated for antenna efficiency and ECC in a reverberation chamber. A low ECC (< 0.2) and more than 65%

efficiency were achieved. The proposed technique could be used effectively through designing a MIMO system with closely spaced antennas in real wireless communication environments.

ACKNOWLEDGMENT

REFERENCES

1. Krairiksh, M., P. Keowsawat, C. Phongcharoenpanich, and S. Kosulvit, "Two-probed excited circular ring antenna for MIMO application," *Progress In Electromagnetics Research*, Vol. 97, 417–431, 2009.
2. Yu, X. H., L. Wang, H.-G. Wang, X. Wu, and Y.-H. Shang, "A novel multiport matching method for maximum capacity of an indoor MIMO system," *Progress In Electromagnetics Research*, Vol. 130, 67–84, 2012.
3. Sharawi, M. S., A. B. Numan, and D. N. Aloi, "Isolation improvement in a dual-band dual-element MIMO antenna system using capacitively loaded loops," *Progress In Electromagnetics Research*, Vol. 134, 247–266, 2013.
4. Tse, D. and P. Viswanath, *Fundamentals of Wireless Communication*, Cambridge University Press, New York, 2005.
5. Lee, J.-H. and C.-C. Cheng, "Spatial correlation of multiple antenna arrays in wireless communication systems," *Progress In Electromagnetics Research*, Vol. 132, 347–368, 2012.
6. Yang, F., "Microstrip antennas integrated with electromagnetic band-gap structures: A low mutual coupling design for array applications," *IEEE Trans. Antennas Propag.*, Vol. 51, No. 10, 2936–2946, 2003.
7. Islam, M. T. and M. S. Alam, "Compact EBG structure for alleviating mutual coupling between patch antenna array elements," *Progress In Electromagnetics Research*, Vol. 137, 425–438, 2013.
8. Chiu, C. Y. and C. H. Cheng, "Reduction of mutual coupling between closely-packed antenna elements," *IEEE Trans. Antennas Propag.*, Vol. 55, No. 6, 1732–1738, 2007.
9. Chou, H. -T., H.-C. Cheng, H.-T. Hsu, and L.-R. Kuo, "Investigations of isolation improvement techniques for multiple input multiple output (MIMO) WLAN portable terminal applications," *Progress In Electromagnetics Research*, Vol. 85, 349–366, 2008.
10. Li, J. F. and Q. X. Chu, "A compact dual-band MIMO antenna of mobile phone," *Journal of Electromagnetic Waves and Applications*, Vol. 25, Nos. 11–12, 1577–1586, 2011.
11. Xiang, Z., X. Quan, and R. Li, "A dual-broadband MIMO antenna system for GSM/ UMTS/LTE and WLAN handsets," *IEEE Antennas Wireless Propag. Lett.*, Vol. 11, 551–554, 2012.
12. Diallo, A. and C. Luxey, "Study and reduction of the mutual coupling between two mobile phone PIFAs operating in the DCS 1800 and UMTS bands," *IEEE Trans. Antennas Propag.*, Vol. 54, No. 11, 3063–3074, 2006.
13. Park, G., M. Kim, T. Yang, J. Byun, and A. S. Kim, "The compact quad-band mobile handset antenna for the LTE 700 MIMO application," *APSURSI'09*, 1–4, Jun. 1–5, 2009.
14. Chung, J. Y., T. Yang, and J. Y. Lee, "Low correlation MIMO antennas with negative group delay," *Progress In Electromagnetics Research C*, Vol. 22, 151–163, 2011.
15. Vongsack, S., C. Phongcharoenpanich, S. Kosulvit, K. Hamamoto, and T. Wakabayash, "Unidirectional antenna using two-probe excited circular ring above square reflector for polarization diversity with high isolation," *Progress In Electromagnetics Research C*, Vol. 133, 159–176, 2013.
16. Xu, H.-X., G.-M. Wang, and M.-Q. Qi, "A miniaturized triple-band metamaterial antenna with radiation pattern selectivity and polarization diversity," *Progress In Electromagnetics Research C*, Vol. 137, 275–292, 2013.
17. Li, W., W. Lin, and G. Yang, "A compact MIMO antenna system design with low correlation from 1710 MHz to 2690 MHz," *Progress In Electromagnetics Research C*, Vol. 144, 59–65, 2014.

18. Coetzee, J. C. and Y. Yantao, "Port decoupling for small antenna arrays by means of an eigenmode feed network," *IEEE Trans. Antennas Propag.*, Vol. 56, No. 6, 1587–1593, 2008.

19. Volmer, C., M. Sengul, J. Weber, R. Stephan, and M. A. Hein, "Broadband decoupling and matching of a superdirective two-port antenna array," *IEEE Antennas Wireless Propag. Lett.*, Vol. 7, 613–616, 2008.

20. Mahmood, F., J.-R. Kazim, M. Karlsson, S. Gong, and Z. Ying, "Decoupling techniques of compact and broadband MIMO antennas for handheld devices," *EuCAP 2012*, 1–5, Mar. 26–30, 2012.

21. Bhatti, R. A. and S. O. Park, "Compact antenna array with port decoupling for LTE-standardized mobile phones," *IEEE Antennas Wireless Propag. Lett.*, Vol. 8, 1430–1433, 2009.

22. Gong, Q., Y.-C. Jiao, and S.-X. Gong, "Compact MIMO antennas using a ring hybrid for WLAN applications," *Journal of Electromagnetic Waves and Applications*, Vol. 25, Nos. 2–3, 431–441, 2011.

23. Chaloupka, H. J. and X. Wang, "Novel approach for diversity and MIMO antennas at small mobile platforms," *PIMRC 2004*, 637–642, Sep. 5–8, 2004.

24. Dossche, S., S. Blanch, and J. Romeu, "Optimum antenna matching to minimize signal correlation on a two port antenna diversity system," *Electron. Lett.*, Vol. 40, No. 19, 1164–1165, 2004.

25. Chen, S. C. and S. J. Chung, "A decoupling technique for increasing the port isolation between two strongly coupled antennas," *IEEE Trans. Antennas Propag.*, Vol. 56, No. 12, 3650–3658, 2008.

26. Cui, S., S.-X. Gong, Y. Liu, W. Jiang, and Y. Guan, "Compact and low coupled monopole antennas for MIMO system applications," *Journal of Electromagnetic Waves and Applications*, Vol. 25, Nos. 5–6, 703–712, 2011.

27. Pozar, D. M., *Microwave Engineering*, 3rd edition, John Wiley, New York, 2005.

28. Balanis, C. A., *Antenna Theory*, 3rd Edition, John Wiley, New York, 2005.

29. An, H., Bart, K. J. C. Nauwelaers, and A. R. Van de Capelle, "Broadband microstrip antenna design with the simplified real frequency technique," *IEEE Trans. Antennas Propag.*, Vol. 42, No. 2, 129–136, 1994.

30. Chen, X., P. Kildal, J. Carlsson, and J. Yang, "Comparison of ergodic capacities from wideband MIMO antenna measurements in reverberation chamber and anechoic chamber," *IEEE Antennas Wireless Propag. Lett.*, Vol. 10, 446–449, 2011.